UAS-based remote sensing applications on the Northern Colorado Limited Irrigation Research Farm

Huihui Zhang*, Kevin Yemoto

(*Water Management and Systems Research Unit, USDA Agricultural Research Service, Fort Collins, Colorado, USA*)

Abstract: USDA-ARS (Agricultural Research Service) Water Management and Systems Research Unit established a Limited Irrigation Research Farm (LIRF) in Northern Colorado in 2008 to respond the urgent need of sustaining irrigated agriculture in semi-area regions with limited water resources and increasing population. Agricultural research has been conducted at this facility to optimize irrigation strategy, accurately quantify crop water use, develop sensor-based irrigation scheduling algorithms, and investigate physiological responses to crop water stress. An unmanned aerial system (UAS) was developed and used to collect multispectral and thermal imagery for irrigation and other field applications. The results in the study confirmed the capability of UAS to collect high-quality, high spatial and temporal resolution crop data for field-based agricultural applications and aid farmers to manage their water resources and sustain crop production in a more advanced way.

Keywords: NDVI, CRSI, CWSI, maize, water stress, genotype, yield

DOI: 10.33440/j.ijpaa.20190202.50.

Citation: Zhang H, Yemoto K. UAS-based remote sensing applications on the Northern Colorado Limited Irrigation Research Farm. Int J Precis Agric Aviat, 2019; 2(2): 1–10.

1 Introduction

Farmers in Northern Colorado and other semi-arid regions globally face a crucial challenge of maintaining crop production in the face of continuously declining irrigation supplies. Water resources initially allocated for agricultural production are increasingly being diverted for municipal, industrial, and environmental uses. Therefore, it is urgent for farmers to improve the tools and practices they use to manage their farms in order to save water and maintain yields to feed an increasing global population, which could hit 9.7 billion in 2050[1].

Maize is a major crop for human consumption and an important feed for livestock both regionally and globally. More irrigated land is planted to maize than any other crop in the U.S., and this trend is increasing[2,3]. Many studies have been conducted on water management strategies that maximize maize production, such as agronomic practices and irrigation systems, and maximize water-use efficiency, such as growth stage-based deficit irrigation[4,5]. In semi-arid Northern Colorado, maize (*Zea mays L.*) is grown mostly under irrigated conditions. Average annual precipitation in the region (2008-2013) was about 197 mm, and average maize crop evapotranspiration (ETc) was 666 mm[6]; thus, irrigation is imperative during the growing season to meet crop water requirement. When irrigation water supplies are limited, producers must consider alternative water management strategies to maintain economic productivity. Many studies have been conducted on water management strategies that maximize maize production[6-9].

Received date: 2019-12-11 **Accepted date:** 2019-12-20

Biography: **Huihui Zhang**, PhD, Research Physical Scientist, research interests: remote sensing, precision agriculture, irrigation management, Email: huihui.zhang@usda.gov; **Kevin Yemoto**, BS, Engineering Technician, research interests: remote sensing, precision agriculture, soil science, GIS, Email: kevin.yemoto@usda.gov. Mailing Address: 2150 Centre Avenue, Bldg. D, STE 320, Fort Collins, Colorado, USA 80526.

*** Corresponding author: Huihui Zhang**, PhD, Telephone number: +01-970-492-7413, Email: huihui.zhang@usda.gov.

USDA-ARS (Agricultural Research Service) Water Management and Systems Research Unit established a Limited Irrigation Research Farm (LIRF) near Greeley, Colorado in 2008 and has been conducting research since then on optimizing water management strategies to sustain irrigated agriculture in semi-arid regions with limited water supplies. Scientific methods were developed to manage irrigation, accurately quantify crop water use, develop sensor-based irrigation scheduling algorithms, and investigate physiological responses to crop water stress[6-19].

Remote sensing technology has been applied in precision agriculture for a few decades. Recent rapid advances in unmanned aerial vehicles (UAVs), sensor technology, image and big-data processing techniques have yielded data with higher spatial and temporal resolution than other remote sensing platforms. As a result, UAV-based remote sensing data and products have the potential to lead precision agricultural management to a higher level that is more affordable, reliable and cost-effective[20-26]. In 2017, we developed a UAV-based multispectral and thermal system (UAS) to collect remote sensing data for irrigation management. In this paper, we reported in detail on how the UAS was utilized on the research farm for irrigation control, crop water-use estimation, crop yield prediction, and other field applications.

2 Material and methods

2.1 ARS Limited Irrigation Research Farm, experimental design, and irrigation management

2.1.1 Experiment site and treatment design

Research was conducted on the Limited Irrigation Research Farm (LIRF) in Greeley, Colorado USA (40°26′53.78″N, 104°38′20.80″W). A 4.7-ha experimental field was divided into 4 equal sections. From 2017-2019, the western two sections and eastern two sections were used to grow maize and sorghum in rotation. Maize was planted in the eastern two sections in 2017 and 2019 and the western two sections in 2018. Each field section was divided into four replicate blocks, and each block was divided into six 9×43 m plots containing 12 N-S oriented crop rows

(0.76 m row spacing) on which six irrigation treatments were randomly assigned (Figure 1). In 2017 two variables (8 genotypes of maize and 3 irrigation treatments) were tested, with the irrigation treatments receiving 100, 70, and 40 percent of full crop evapotranspiration (ETc). There was a total of 96 plots where traditional maize genotypes A, B, E, and H were planted on the north side and drought-tolerant maize genotypes C, D, F, and G were planted on the south side. The commercial codes of these Syngenta maize genotypes A-H are N68B, N47L, N59B, N68K, G10D98, G12J11, N70M, G09H57, respectively.

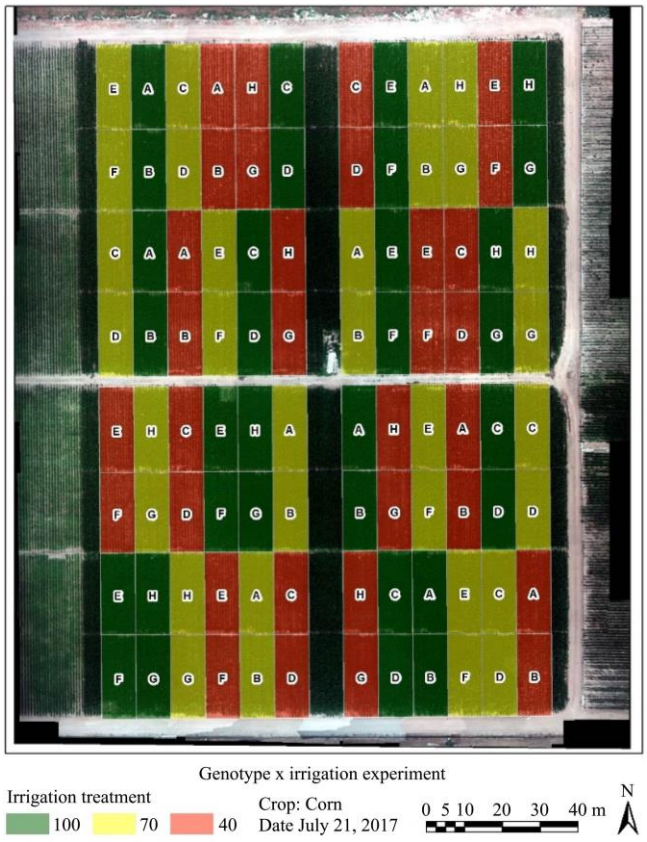

Figure 1 Experimental design with 8 maize genotypes and 3 levels of irrigation on the Limited Irrigation Research Farm. Genotypes A-H are N68B, N47L, N59B, N68K, G10D98, G12J11, N70M, G09H57, respectively. Color code represents irrigation treatments: 100% of ETc (green), 70% of ETc (yellow), and 40% of ETc (red)

Irrigation water from a groundwater well was delivered to the end of each plot through underground PVC pipe and applied to each crop row through surface drip irrigation tubing with 30-cm in-line emitter spacing (1.1 L h^{-1} per emitter). The east and west edges of each crop section contained a 6-row buffer, with all measurements taking place in the middle 4 to 6 rows. Irrigation applications were measured independently for each treatment with turbine flowmeters (Badger Record all Turbo 160 with RTR transmitters, Badger Meter, Milwaukee, Wisconsin), which were cross calibrated to ensure accuracy and consistency. Irrigation applications were controlled by and recorded with Campbell Scientific CR1000 data loggers (Campbell Scientific, Logan, UT, USA). Maize was planted on May 4, 2017, at a seeding rate of 86,500 seeds ha^{-1} and resulted in a final population of 74,647 plants per ha. Fertilizers were applied at planting and in-season with the irrigation water to avoid nutrient deficiencies on all treatments.

The three irrigation treatments with varying levels of deficit irrigation were arranged in a randomized block design with four replications. Deficit irrigation was applied during the late vegetative (V8~VT) and maturation (R4~R6) growth stages[7,8]. The full irrigation treatment was targeted to meet potential non-stressed crop ETc, as predicted by the reference evapotranspiration (ETr) and crop coefficients from FAO-56 methodology[27,28]. The 70% and 40% irrigation treatments were irrigated with 70 and 40 percent of fully irrigated treatment during late vegetative and maturation stages. All treatments received 100% ETc from planting through V7, and during the reproductive (VT to R4) growth stage.

2.1.2 Irrigation control and water balance

Meteorological data were taken by an on-site Colorado Agricultural Meteorological Network (CoAgMet, http://ccc.atmos.colostate.edu/~coagmet/) station GLY04. These data include hourly precipitation, air temperature, relative humidity (and subsequent vapor pressure deficit), solar radiation, and wind speed taken at 2 m above a grass reference surface. Alfalfa-based ETr was calculated from hourly weather data by the ASCE standardized Penman-Monteith equation[27], and daily values are sums of hourly values.

An access tube installed in the middle row of each plot was used to determine soil water content (SWC) by a neutron moisture meter (CPN-503 Hydroprobe, InstroTek, San Francisco, CA, USA). The SWC was measured at depths of 30, 60, and 90 cm, 2 or 3 times per week before or after irrigation in each northside plot where genotypes A, C, E and H were planted. SWC of the 0 to 15 cm layer was measured with a portable time domain reflectometer (MiniTrace, Soil Moisture Equipment Corp, Santa Barbara, CA) in the row near the neutron moisture meter access tube. Field capacities from each layer were estimated based on observations of SWC from the current season and the previous 5 years of study on the site. The soil water deficit (SWD) for the active root zone of each plot was calculated by sum of the difference between SWC and field capacities in each layer, normalized by layer thickness. Soil water storage changes (ΔS) were calculated by a soil water balance, with precipitation (P) and irrigation (I) as water inputs, and runoff (RO), deep percolation (DP) and evapotranspiration (ETc) as water outputs ($\Delta S = P + I - RO - DP - ETc$). For the experimental field, RO was assumed zero due to relatively small field slope and precipitation amounts, adequate soil infiltration and surface residue, and controlled drip irrigation. Deep percolation was assumed to occur when precipitation exceeded the SWD in the full root zone (105 cm) at the time of precipitation and was calculated as the precipitation amount minus soil water deficit ($DP = P - SWD$). For other days, a daily time-step soil-water balance model was developed based on the FAO-56 dual crop coefficient approach [28] to estimate daily ETc. The model was based on alfalfa reference ETr and initial and full-cover basal crop coefficients (K_{cb}), respectively[29], and adjusted for measured crop canopy growth and senescence. Based on the full season correlation between factional canopy cover (f_c) and K_{cb} reported by[11], where $K_{cb} = 1.05$ for $f_c > 0.8$ and $K_{cb} = 1.10 f_c + 0.17$ for $f_c < 0.8$ (initial- and mid-season). The model estimated the daily ETc (including soil evaporation and transpiration), DP, and SWD. More details on soil water balance calculation can be referred to[17].

2.1.3 Plant measurements

Canopy cover f_c was measured in the center of each plot approximately weekly near solar noon by the UAS from a nadir view 15 m above the ground surface (see section 2.2). The digital image pixels were differentiated between green plant canopy and background (soil, surface residue, and senesced leaves) with an

in-house developed image analysis method in Python 3.5.3.

In the FAO-56 dual crop coefficient methodology[28], ETc = (K_{cb}*K_s + K_e)*ETr. Here, the K_{cb} is defined as the ratio between crop potential transpiration and alfalfa-based reference ETr and used to determine crop potential transpiration under well-watered conditions. For crop under water-limited conditions, actual transpiration will be limited by soil water supply, so the water stress coefficient (K_s) will multiply K_{cb} to account for the influence of water stress on crop transpiration. K_e is a wet soil evaporation coefficient. Traditionally K_s was calculated using FAO-56 soil water depletion method using equation $(TAW - D_r)/(TAW - RAW)$, where TAW is the total available soil water in the root zone (mm), D_r is the root zone depletion (mm), and RAW is the readily available water (mm). In this study, we used a canopy temperature derived crop water stress index (CWSI) to determine the stress coefficient as $K_s = 1 - CWSI$. Canopy temperature was measured using the UAS (see section 2.2). CWSI was calculated using the method given in Han et al.[17], with empirical-model estimate of non-transpiring and full transpiring conditions.

Whole-plant transpiration (i.e., sap flow) was measured on two plants per plot from genotypes A, C, E and H in 100% and 40% treatments with stem heat balance sap flow EXO sensors (Dynamax, Inc, Houston, TX, USA)[30], thus a total of eight sensors were installed for each treatment. Continuous data were collected at 15-minute interval and converted to hourly data from late Jul to Sep in 2017. More details on sap flow measurements can be found in[17].

Grain was harvested on Nov 9, 2017, from each plot (20.7× 6.1 m^2) using a 4-row combine with an active yield monitor. Each plot had two passes of the combine of 4 rows each pass. A weigh wagon was used to record each pass and replicates. Grain was threshed with a stationary thresher (Wintersteiger Classic ST, Wintersteiger AG, Ried, Austria), weighed and subsampled for moisture content determination. Grain moisture content at harvest was measured with a Dickey-john GAC500-XT Moisture Tester (Dickey-john Corp, Aubern, IL, USA). Yield (kg/ha) was normalized to 15.5% moisture content (commercial yield standard).

2.1.4 Transpiration estimation

Crop transpiration was estimated using two methods based on data described in sections 2.1.2 and 2.1.3. The UAS method estimated crop transpiration as K_{cb}*K_s*ETr. The K_{cb} coefficient was 1.10 f_c + 0.17 (or 1.05 for f_c > 0.8), and Ks coefficient was estimated as 1–CWSI, with CWSI calculated using canopy temperature derived from UAV data (FLIR Tau2 LWIR). The water balance (WB) method neglected soil evaporation for full-canopy conditions, resulting in crop transpiration estimated as ETc = (I + P – ΔS – DP). On days with no I, P, or DP, ETc is simply –ΔS, which is determined as the 24-hour change of depth-weighted average of soil moisture measurements from both TDR (0-15 cm) and neutron probe (15-90 cm).

2.1.5 Soil survey

The largest portion of the field experimental area contains Olney fine sandy loam soil (fine-loamy, mixed, superactive, mesic Ustic Haplargids). Other soils in the field are Nunn clay loam (fine, smectitic, mesic Aridic Argiustolls) in the southeastern section[31]. Apparent electrical conductivity (ECa) survey of the field was conducted via a Veris 3100 (Veris Technologies, Salina, KS). The Veris 3100 measures ECa as a voltage drop across a pair of coulter-electrodes. Two EC arrays allow for mapping ECa to depth ranges of 0-30 cm and 0-90 cm (Figure 2). Scudiero et al.[32] has developed a method to use satellite canopy reflectance to assess soil salinity at reginal scale. In this study, the canopy response salinity index (CRSI) [32] was tested to estimate crop yield due to the soil variability.

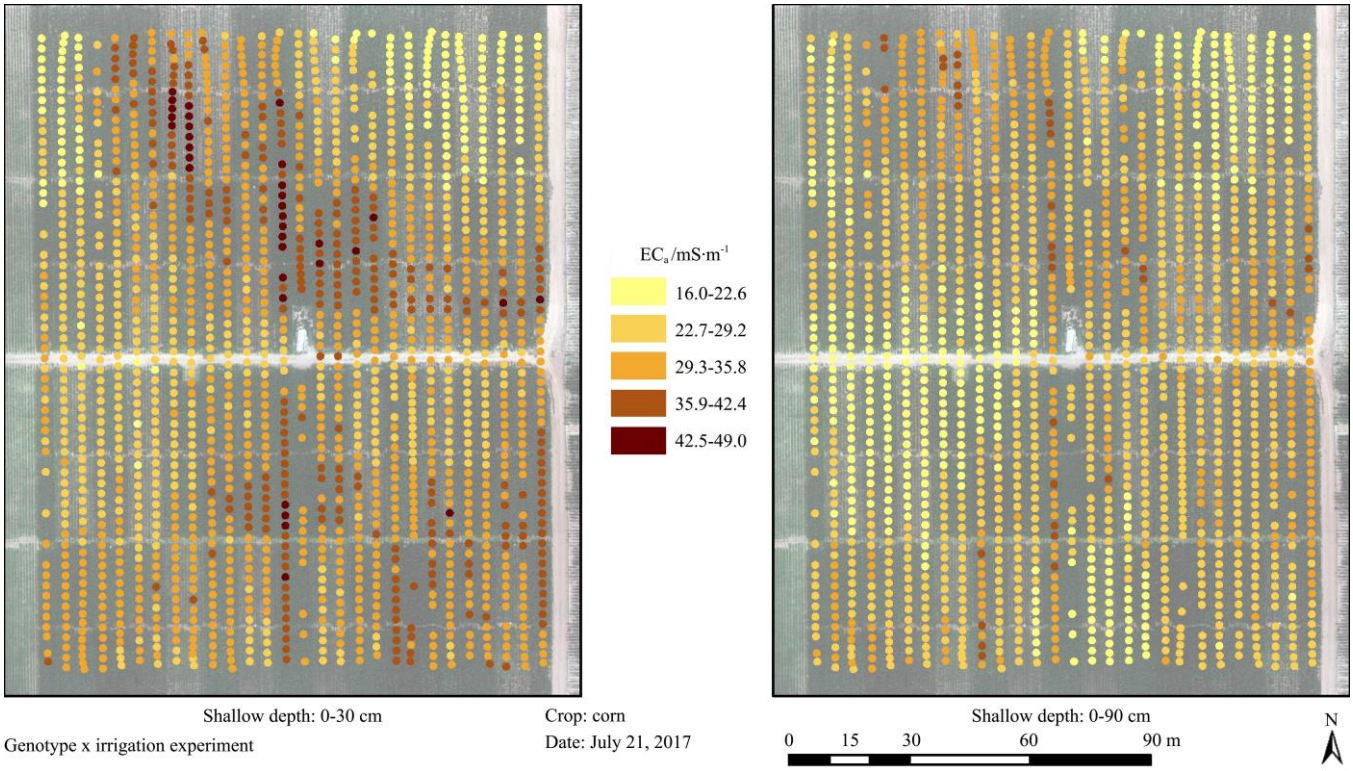

Figure 2 ECa survey of field conducted in 2012 with Veris 3100. ECa maps are split into 2 depths 0-30 cm (left) and 0-90 cm (right)

2.2 Unmanned aerial system

2.2.1 Unmanned aerial vehicle and payload

The UAV platform is a DJI Spreading Wings S900 hexacopter (Da-Jiang Innovations Science and Technology Co., LTD, Shenzhen, China) with 3DR Pixhawk PX4 flight controller/autopilot (3D Robotics, Berkley, CA). The payload for

the UAS consists of a FLIR Tau2 LWIR (FLIR Systems, Inc., Wilsonville, OR) and Tetracam Mini-MCA6 multispectral cameras (Tetracam Inc., Chatsworth, CA). The custom carbon fiber mounting tray for the payload was designed and built by UASUSA (UASUSA, Longmont, CO). The Tau2 contains a 640×480-pixel (0.3 megapixel) image sensor and has a spectral range from 7.5 to 13.5 μm. The Mini-MCA6 features a 6-camera array, with each camera containing 1280×1024-pixel (1.3 megapixel) image sensor. Each of the 6 cameras is fitted with a band-pass filter with 10 nm bandwidth. The center wavelength of filters used in the study were 860, 720, 680, 570, 530, and 490 nm.

2.2.2 Image acquisition

To ensure a common exposure setting across flights, the camera shutter speed was set/locked pre-flight using an 18% reflectance target. The shutter speed setting was maintained throughout flight mission; however, the setting was reset in the event of environmental or temporal changes between multiple flight missions. Flight missions were separated into low-altitude high-resolution plot to plot mission suitable for canopy cover measurements and high-altitude fly missions suitable for orthomosaics.

Canopy cover missions were flown at 15 m above ground level (AGL) which gives a pixel resolution of 0.8 cm and an image footprint of 10.4×8.3 m. The missions were programed with waypoints above the center of each plot, with the UAV orientation locked so the vehicle always faced toward east. At each waypoint the UAV was set to hover pre and post image acquisition to ensure high quality images free of motion blur and orientation bias. Flights were conducted at 11:00AM with the field split into two 10-minute missions.

Orthomosaic missions were flown at 70 m AGL which gives a pixel resolution of 3.79 cm, with an image footprint of 48.6 m× 38.3 m. The missions were programed to fly north-south with the UAV orientation locked so the vehicle always faced toward north. Waypoints were programed to have an image overlap of 90% and 70% sidelap with a low flight speed around 1.5 m/sec to minimize motion blur. The flight pattern over the study site was split into two missions with one transect of overlap between the two missions. Flights were conducted at 12:00PM, with each mission taking about 11 minutes.

2.2.3 Ground truth

For each flight, pre- and post-flight images of a set of reflectance targets were taken. Images of three reflectance targets (99%, 50% and 10% Labsphere Spectralon targets; Labsphere, Inc., North Sutton, NH, USA) were taken at altitude. Spectroradiometer ground truth measurements of the reflectance targets were also taken pre and post flight using Spectral Evolution PSR-1100 sepctroradiometer (Spectral Evolution, Lawrence, MA, USA). The images of the reflectance targets were used to create a calibration curve to convert the multispectral images from digital numbers (DNs) to reflectance. Aside from the set of reflectance targets, five 45×45 cm ground control panels were strategically placed across the field and located using Trimble GPS (Trimble Inc., Sunnyvale, CA, USA). The ground control points were used to increase positional accuracy of completed orthomosaics.

2.2.4 Image processing

The 6-band multispectral images were registered using PixelWrench 2 software (Tetracam Inc., Chatsworth, CA, USA) to create multipage Tiff files. Spectroradiometer data were downloaded and processed using DARWin SP Data Acquisition and Analysis software (Spectral Evolution, Lawrence, MA, USA). As the spectroradiometer has a bandwidth of 1.5 nm, the average readings around the center wavelength of each filter were calculated. GPS coordinates were extracted from the Pixhawk telemetry flash log. The autopilot adds a 1-second delay to CAM message; therefore, to improve accuracy of GPS location corresponding to image location, 1-second was subtracted from CAM message timestamp, and the coordinates associated to the closest GPS timestamp was used. The 6-band multispectral orthomosaic was created using Icaros OneButton Professional 5.1 (Icaros US, Manassas, VA, USA). Using ESRI ArcGIS 10.4 (ESRI, Redlands, CA, USA), the multispectral images of the reflectance targets were sampled for each band. The sampled area for each reflectance target was the same, with the sample area taken from the center of each reflectance panel. The sampled points from the multispectral images and the calculated reflectance values from the spectroradiometer were used to create a linear equation for each band to convert raw digital numbers to reflectance values.

Various vegetative indices (VIs), such as normalized difference vegetation index (NDVI)[33], soil-adjusted vegetation index (SAVI)[34], transformed chlorophyll absorption in reflectance index (TCARI)[35], and CRSI[32], were calculated from 6-band reflectance images in ArcGIS using the following equations (1) – (4):

$$NDVI = \frac{NIR - R}{NIR + R} \tag{1}$$

$$SAVI = \frac{(1+L)(NIR - R)}{NIR + R + L} \tag{2}$$

$$TCARI = 3\left[(RE - R) - 0.2(RE - G)\left(\frac{RE}{R}\right)\right] \tag{3}$$

$$CRSI = \sqrt{\frac{(NIR * R) - (G * B)}{(NIR * R) + (G * B)}} \tag{4}$$

where, *NIR* is near infrared (860 nm band) reflectance; *R* is red (680 nm band) reflectance; *L* is a canopy background adjustment factor; *RE* is red edge (720 nm band) reflectance, and *G* is green (530 nm band) reflectance, and *B* is blue (490 nm band) reflectance.

2.3 Statistical analysis

Ordinary least square linear regression was performed to determine the relationship between dependent and independent variables. The fitting quality of the model was evaluated by the adjusted coefficient of determination (R^2_adj), and Root Mean Square Error (RMSE, eq. (5)).

$$\mathrm{RMSE} = \sqrt{\frac{1}{n}\sum_{i=1}^{n}(P_i - O_i)^2} \tag{5}$$

where, P_i is the predicted value; O_i is the observed value; $\bar{O}$ and $\bar{P}$ are the mean observed and predicted values, respectively, and n is the number of data pairs. The statistical analyses were conducted in JMP 11 (JMP software, Cary, NC)

3 Results and Discussion

3.1 Fractional canopy cover, crop coefficient, and crop transpiration

Plot level UAS images were taken from four genotypes (A, C, E, and H) in three irrigation treatment plots (40, 70, and 100% ETc) to measure fractional canopy cover, f_c. All 100% of ETc treatments reached full canopy cover around 83 days after planting (DAP), but f_c values in 70% and 40% of ETc treatments were about 5% and 20% less than those for fully irrigated crops, respectively

(Figure 3). Among the four genotypes under 40% of ETc treatment, genotype E had the smallest canopy cover, followed by drought-tolerant genotype C. Although all plots reached reproductive R1 stage at the same day (DAP 90), water stress slowed the process to reach full canopy cover, decreased the f_c at full canopy cover, and sped up the process of senescence in the late season. Figure 4 shows the K_{cb} curves derived from f_c. When f_c was greater than 80%, constant K_{cb} value 1.05 was used for the mid-season. Additional canopy during the mid-season did not significantly improve transpiration[11].

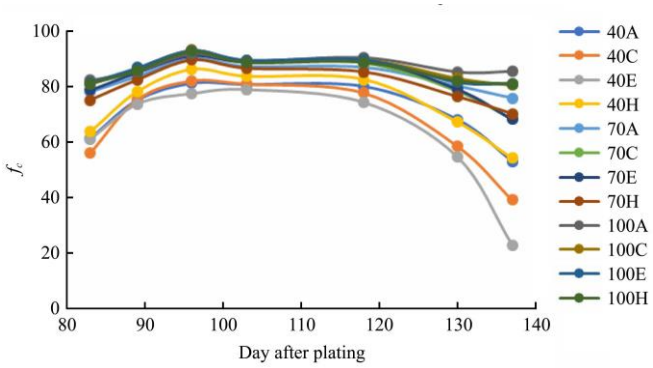

Figure 3 Fractional canopy cover (f_c) derived from UAS imagery taken in the 2017 growing season. Lines labeled by irrigation level (40, 70, 100% of ETc) and genotype (A, C, E, H)

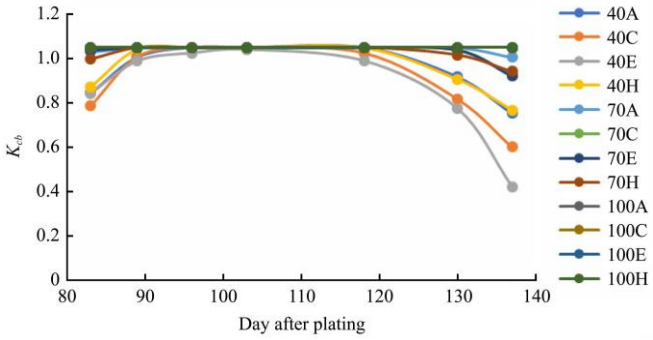

Figure 4 Crop coefficient (K_{cb}) estimated from fractional canopy cover (f_c) in the 2017 growing season. Lines labeled by irrigation level (40, 70, 100% of ETc) and genotype (A, C, E, H)

The daily crop transpiration was calculated as ETr multiplied by (1 – CWSI) and K_{cb}, where ETr was taken from weather station and CWSI and K_{cb} were derived from UAS images. The results were compared with daily sap flow data on Aug 30 and Sep 11, 2017. Figure 5 shows transpiration derived by UAS images or soil water balance model compared to the sap flow measurement. The UAS-derived crop transpiration had better performance than those calculated by soil water balance model with higher adjusted R^2 and smaller RMSE. Soil water balance model predicted lower transpiration for stressed plants, but UAS derived transpiration was higher than sap flow measurements for fully irrigated crops.

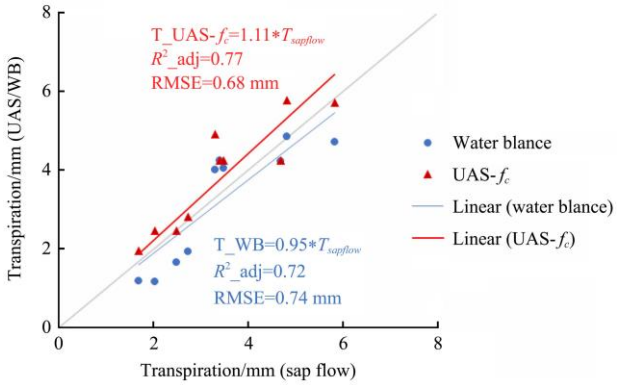

Figure 5 Correlation between plant transpiration estimates derived from sap flow measurement versus UAS or soil water balance (WB) methods (data includes measurements from genotypes A, C, and H under 100% and 40% of ETc treatments on Aug 30 and Sep 11, 2017)

3.2 Time series of VI images and crop yield

Orthomosaic missions were completed on Jul 21 (late vegetative stage), Aug 30 (reproductive stage) and Oct 16, 2017 (maturation stage). Figure 6 shows NDVI and CRSI images acquired over all the plots. 40% of ETc treatment plots can be differentiated from other treatments with lighter pixel color on Jul 21. All plots were fully irrigated during reproductive stage, so the NDVI and CRSI images on Aug 30 show more homogeneous color over the plots. The maximum VI values were obtained from fully irrigated treatments for all genotypes.

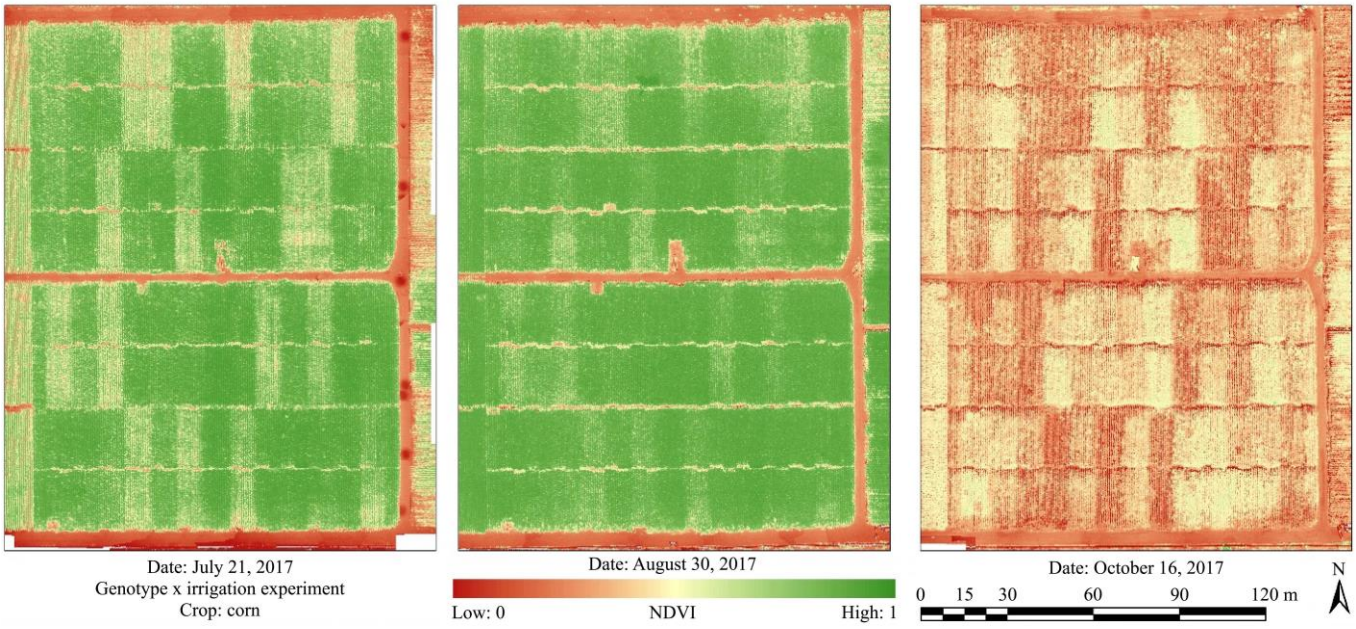

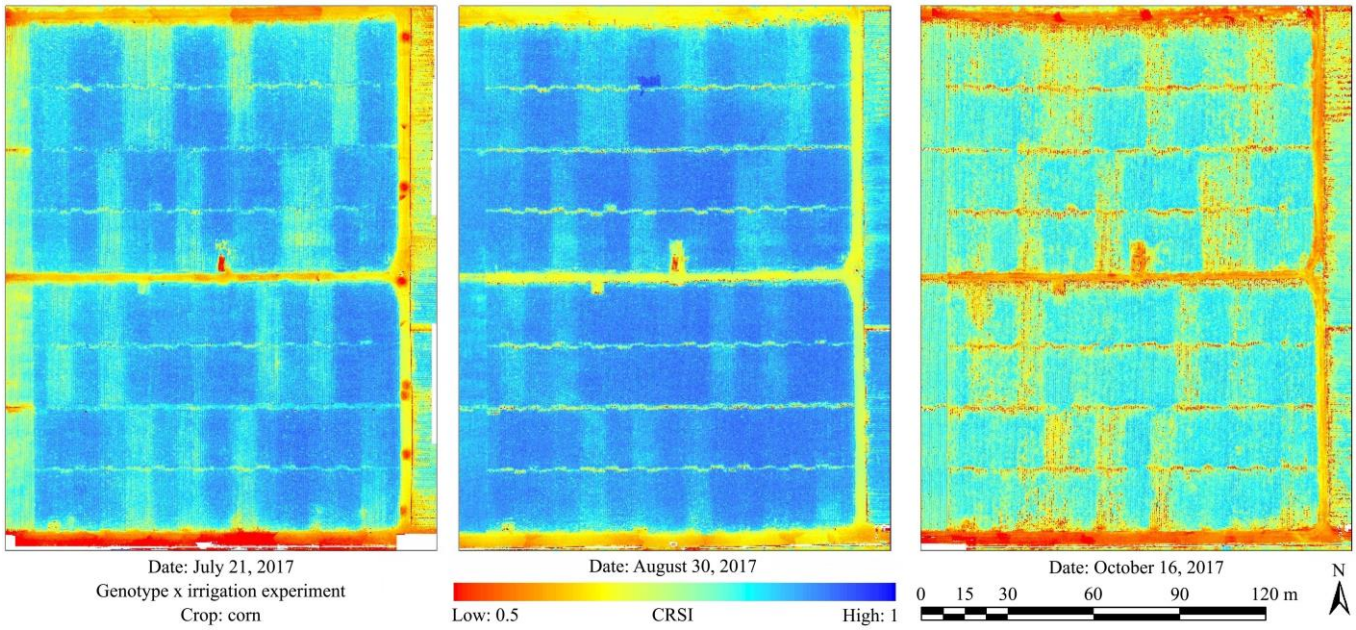

Figure 6 Orthomosaics UAS NDVI and CRSI images acquired on Jul 21, Aug 30 and Oct 16, 2017 over the experimental site at LIRF

The average maize yield and VI on different days (Jul 21, Aug 30, Oct 16) were obtained for each treatment to determine the accuracy of using VIs for yield estimation. Table 1 shows the best result of linear regression on Jul 21 was NDVI, with higher R^2 of 0.826 and smaller RMSE of 1414 kg/ha than the other VIs. However, later in the season, CRSI had better performance than the other VIs, which confirmed soil EC variation in the field could have impact on grain yield. TCARI was better than NDVI at the reproductive stage but performed poorly at the maturation stage. The reason for this is that TACRI was designed to be more sensitive to leaf chlorophyll content[35]. Leaves with a higher concentration of chlorophyll have a direct correlation with grain yield, and water stress decreased chlorophyll content in the leaves[36]. The RMSE of all VIs increased with time except for SAVI. Overall, all regression models were statistically significant (p<0.05) for the estimation of maize yield. The highest accuracy of the models was NDVI at the late vegetative stage or CRSI at the reproductive and maturation stage.

Table 1 Adjusted coefficients of determination (R^2) and RMSE (kg/ha, in parentheses) in estimating yield with vegetation indices, NDVI, SAVI, TCARI, and CRSI, based on measurements during late vegetative (Jul 21), reproductive (Aug 30), and maturation (Oct 16) growth stages

Vegetation Index	Jul 21, 2017	Aug 30, 2017	Oct 16, 2017
NDVI	0.826 (1414.0)	0.700 (1858.9)	0.677 (1929.1)
SAVI	0.800 (1517.7)	0.572 (2219.7)	0.674 (1938.6)
TCARI	0.787 (1566.7)	0.765 (1643.8)	0.312 (2815.6)
CRSI	0.805 (1498.4)	0.773 (1618.0)	0.739 (1735.0)

The yield to NDVI and CRSI relationships were also evaluated for all genotypes. Table 2 shows again CRSI performed better than NDVI at the reproductive and maturation stage except for genotype G and genotype A on Aug 30. Among genotypes, CRSI of genotypes B, D, E and F had higher R^2 and smaller RMSE than the other genotypes, and were close to NDVI on Jul 21 and better than NDVI on Aug 30 and Oct 16.

3.3 Other applications

3.3.1 Drip line leaking detection

Orthomosaics of another irrigation experimental field south of

Table 2 Adjusted coefficients of determination (R^2) and RMSE (kg/hm^2, in parentheses) in estimating yield with vegetation indices, NDVI and CRSI for 8 maize genotypes A-H (N68B, N47L, N59B, N68K, G10D98, G12J11, N70M, G09H57, respectively) based on measurements during late vegetative (Jul 21), reproductive (Aug 30), and maturation (Oct 16) growth stages

Genotype	Drought-tolerant	NDVI	CRSI
		Jul 21, 2017	
A	N	0.737 (2471.7)	0.731 (2497.8)
B	N	0.936 (769.5)	0.895 (985.6)
C	Y	0.843 (1562.1)	0.802 (1753.9)
D	Y	0.934 (810.2)	0.954 (675.9)
E	N	0.937 (935.6)	0.937 (932.8)
F	Y	0.90 (1111.6)	0.878 (1213.0)
G	Y	0.507 (2004.1)	0.423 (2166.9)
H	N	0.845 (1290.5)	0.751 (1637.3)
		Aug 30, 2017	
A	N	0.604 (3032.7)	0.764 (2340.4)
B	N	0.821 (1289.12	0.925 (833.4)
C	Y	0.706 (2134.4)	0.783 (1832.7)
D	Y	0.894 (1028.4)	0.924 (868.2)
E	N	0.713 (1997.3)	0.807 (1639.0)
F	Y	0.900 (1107.6)	0.904 (1074.5)
G	Y	0.511 (1994.4)	0.470 (2076.7)
H	N	0.730 (1704.8)	0.731 (1702.2)
		Oct 16, 2017	
A	N	0.828 (1995.8)	0.791 (2201.9)
B	N	0.832 (1250.2)	0.874 (1083.2)
C	Y	0.488 (2815.7)	0.639 (2364.9)
D	Y	0.842 (1253.6)	0.890 (1046.0)
E	N	0.848 (1453.9)	0.907 (1136.0)
F	Y	0.792 (1580.9)	0.942 (838.1)
G	Y	0.397 (2215.5)	0.364 (2274.7)
H	N	0.417 (2506.9)	0.531 (2246.9)

the maize plot areas at LIRF were acquired during a post-irrigation leak test to determine if leaks of sub-surface drip lines could be spotted from UAS. Figure 7 shows thermal (7.5 to 13.5 μm) and false-color red edge (or CRE is depicted with the 720 nm as Red, 680 nm as Green, and 530 nm as Blue) imagery of leaks in buried drip lines. The thermal image shows relative temperature changes and can highlight relative cold spots in the field. Used alone, thermal imagery had difficulty detecting differences between irrigation leaks and vegetation unless the leak was large. By adding a false color multispectral (red edge) image, differentiation between irrigation leaks and vegetation patches (in this case a weed patch) becomes more apparent. Relative cold spots and lack of coloration due to vegetation combine to increase the likelihood of standing water or leak.

Concerns: As stated, leaks in buried drip lines can be detected using thermal imagery. However, to help differentiate between leaks and vegetation, it is beneficial to use a false color image in conjunction with thermal imagery. Similarly, if the crop is at a later growth stage, differentiating between a leak and high-transpiration crop may prove to be difficult.

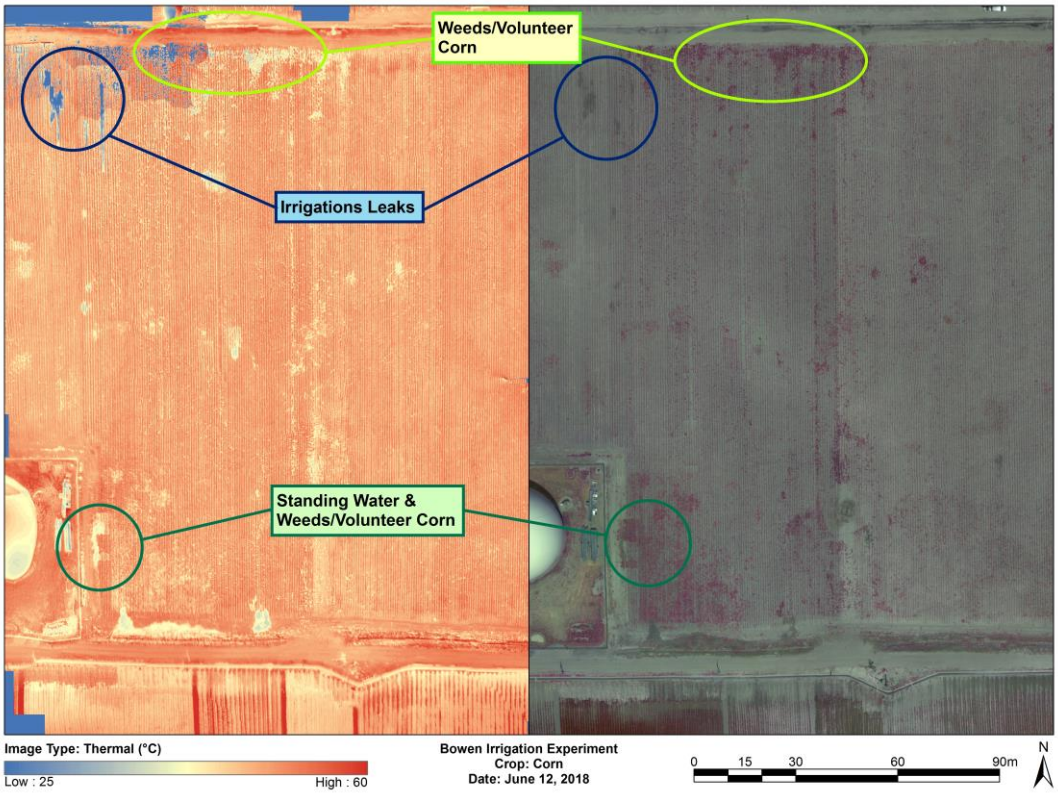

Figure 7 Thermal (7.5-13.5 μm) and false color CRE (720 nm as Red, 680 nm as Green, and 530 nm as Blue) images taken by the UAS over an irrigation experimental field during a post-irrigation leak test on Jun 12, 2018

3.3.2 Hail damage assessment

Figure 8 shows false color infrared (or CIR is depicted with the 860 nm as Red, 680 nm as Green, and 530 nm as Blue) UAS images over a fully irrigated maize plot before (left, taken on Sep 10, 2019) and after (right, taken on Sep 13, 2019) a hail event that occurred in the late evening and early morning of Sep 10/11. Maize plants were in the R5 (kernel dent) growth stage. Comparing canopy cover before and after the hail event indicates a 17.3% reduction of canopy vegetation. The impact of hail damage on yield could be determined by missing vegetation (i.e., missing stands or reduced canopy), growth stage of the crop, and possible damage to cob. For example, according to[37], the yield lost could range from 0-2%.

Concerns: UAS can be used to calculate missing vegetation provided that pre- and post-hail event images were collected. Many canopy cover calculations evaluate for green pixels in the image, which could make differentiating between canopy and leaf litter difficult. This problem can be mitigated by using 3D point cloud analysis to determine vegetation loss. Assessing damage to cobs via UAS would be difficult.

3.3.3 Nutrient deficiency assessment

Figure 9 shows false color CIR, RGB and false color CRE orthomosaic of genotype by irrigation experiment exhibiting signs of chlorosis taken Aug 15, 2018. Chlorosis, or yellowing of leaves due to lack of chlorophyll, can be a sign of nutrient deficiency.

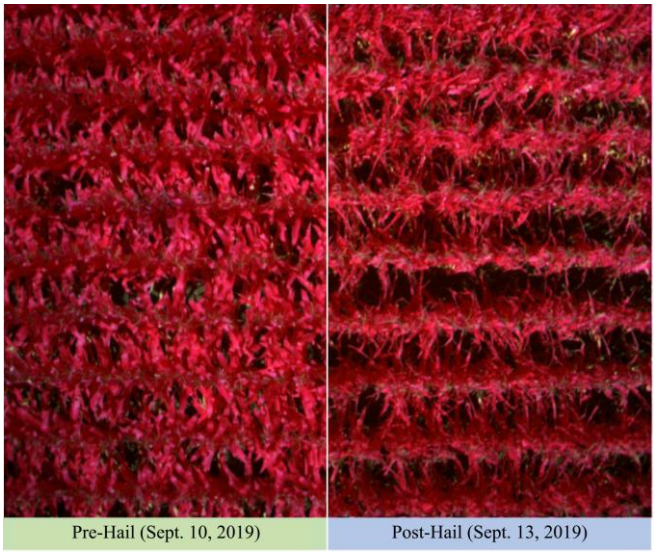

Figure 8 False color CIR images were taken by the UAS over a fully irrigated maize plot before (left) and after (right) a hail event on Sep 10, 2019

Chlorosis initially in younger leaves that spreads to older leaves is an indicator of iron deficiency, whereas the reverse can be an indicator of manganese, zinc, or nitrogen deficiencies. Orthomosaics were created to determine plots that exhibit sign of chlorosis. Plots showing signs of chlorosis were re-flown at a lower altitude for high-resolution imagery; an example is shown in Figure 10. From the high-resolution imagery, it was determined that the younger leaves exhibited signs first, indicating an iron deficiency.

Concerns: From Figure 9, plots affected by chlorosis in false color CIR imagery was not apparent in false color CRE or RGB images, indicating CIR imagery is a poor choice in determining chlorosis in plants. Early detection of nutrient deficiencies is paramount to treatment. Detecting chlorosis in older leaves first via aerial imagery in full canopy may prove difficult.

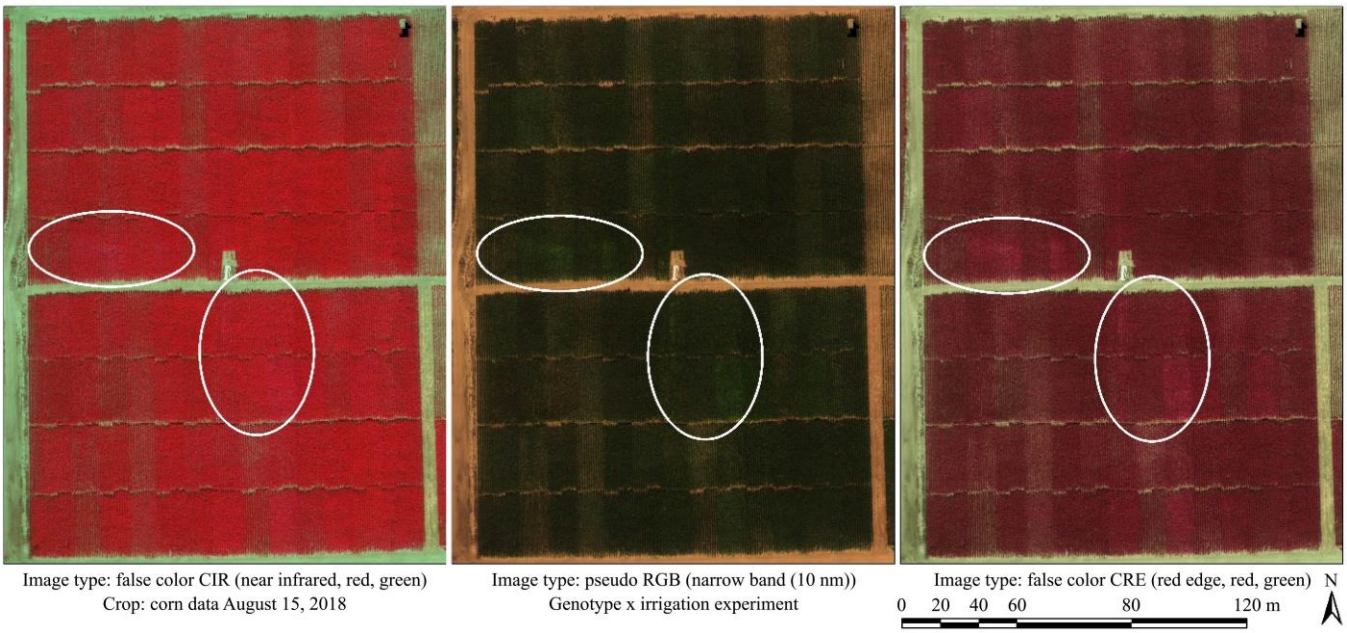

Figure 9 False color CIR, RGB and false color CRE orthomosaics of genotype by irrigation experiment on Aug 15, 2018. Vegetation in false color imagery shows up in red. Vegetation in Circled areas show plots showing signs of chlorosis. Note that in CIR image the plots showing signs of chlorosis is difficult to differentiate from healthy canopy

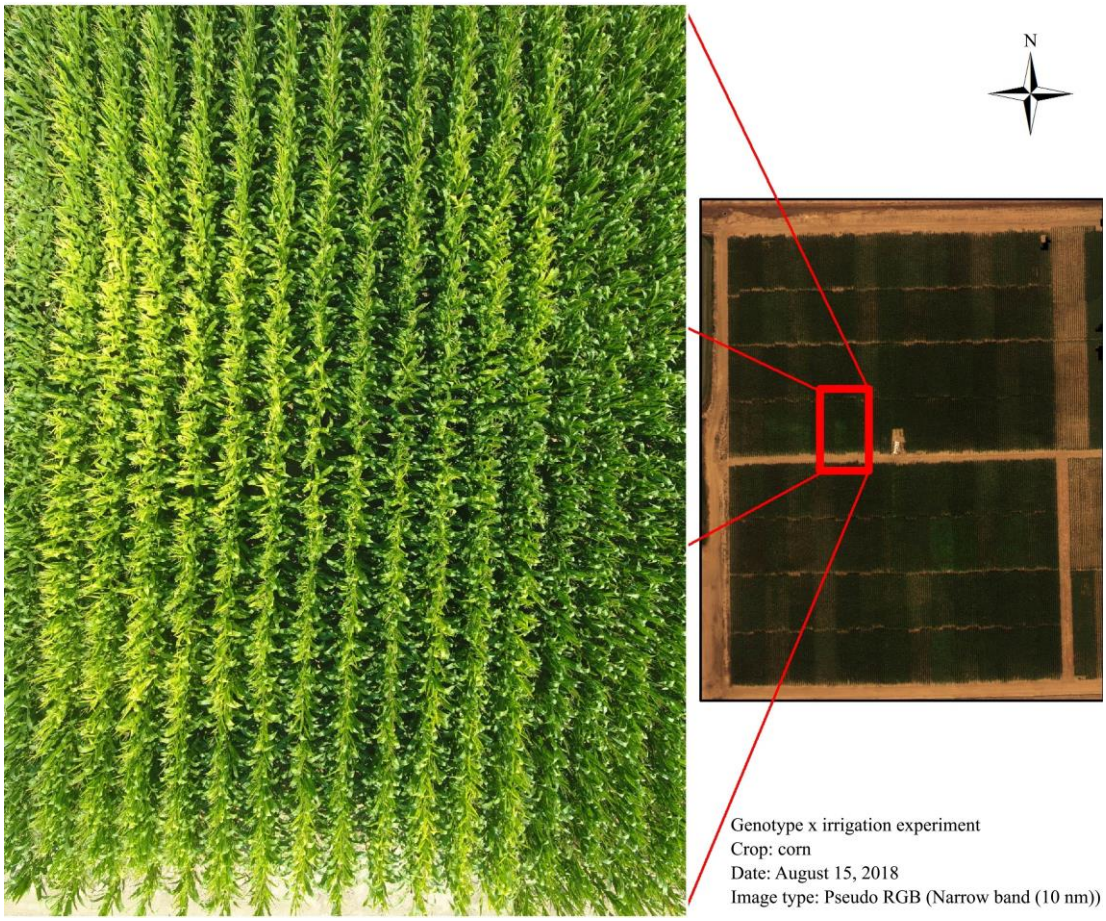

Figure 10 High resolution RGB image of maize plot showing signs of chlorosis on Aug 15, 2018

4 Preflight and safety

Planning is required prior to heading to the field site. Airspace class and proximity to airports of the proposed flight area must be checked. When appropriate, permissions and/or notifications to use airspace must be secured/given prior to missions. Waypoint missions of the study site are built beforehand to allow downtime between flights to be minimized and allow data collection to occur in optimum temporal windows (e.g., wind, solar incidence angle, crop water status). Weather conditions and flight restriction of the proposed area should also be checked prior to flights to ensure conditions are favorable for flights, and that the area is clear of restrictions. The flight team is comprised of 2 certified remote pilots, one acting as pilot in command/visual observer (PIC), the other acting as pilot at controls (PAC). A third team member takes ground truthing measurement and intermittently acts as a second visual observer. The PIC makes final decisions and is ultimately responsible for the flight. The PAC handles manual control of the UAV for the mission. The pilot's roles are decided and assigned before flights occur. The visual observer monitors the sky for hazards and relays information to pilots.

A preflight briefing and inspection of the UAV and flight equipment is performed by the PIC before every flight. On-site weather conditions are monitored using Kestral 5500 weather meter (Kestrel Meters, Boothwyn, PA, USA) and air traffic is monitored using Yaesu FTA-550L Pro-x air band transceiver (Yaesu Musen Co., Ltd., Tokyo, Japan). For this study, a maximum sustained windspeed of 13 mph (20.9 kph) and minimum visibility of 5 statute miles (8.05 km) was set as the threshold for safe minimums. The UAV was powered-on with motors unarmed to warm up the FLIR camera for 25 minutes.

5 Conclusions

The paper reported that Agricultural Research Service Water Management and Systems Research Unit conducted research on using unmanned aerial systems (UAS) for irrigation and field management. The results show use of UAS to be very promising for collecting high quality, high temporal and spatial resolution data, such as canopy cover, vegetation indices, and surface temperature, to estimate crop coefficient, crop water use, water stress, yield, as well as other crop, canopy, and field conditions. In the future, the research team will continue to develop reliable UAS-based remote sensing tools to improve water management in irrigated agriculture.

Acknowledgements

The authors are thankful to the following individual for the support received and for their involvement: Dr. Kendall DeJonge, Dr. Louise Comas, Dr. Sean Gleason, Joe Miller, Brianna Trotter, Cullen McGovern, Garrett Banks, Ross Steward, Alex Mikitowicz, Gerald Buchleiter, Jon Altenhofen.

[References]

[1] United Nations, World Population Prospects 2019: Highlights.

[2] Derner J, Joyce L, Guerrero R, Steele R. 2015. In: Anderson, T. (Ed.), Northern plains regional climate hub assessment of climate change vulnerability and adaptation and mitigation Strategies. USDA, pp. 57.

[3] Wright C K, Wimberly M C. Recent land use change in the Western Corn Belt threatens grasslands and wetlands. P Natl Acad Sci USA, 2013; 110(10): 4134–9.

[4] Kirda C. Deficit irrigation scheduling based on plant growth stages showing water stress tolerance. Food and Agricultural Organization of the United Nations, Deficit Irrigation Practices, Water Reports 2002; 22: 102.

[5] Walthall C, Hatfield J, Marshall E, Lengnick L, Backlund P, Adkins S, et al. Climate Change and Agriculture: Effects and Adaptation. USDA Technical Bulletin 1935. 2013; Washington, DC.

[6] Trout T J, DeJonge K C. Water productivity of maize in the US high plains. Irrigation Science, 2017; 35(3): 251–66.

[7] Comas L H, Trout T J, DeJonge K C, Zhang H, Gleason S M. Water productivity under strategic growth stage-based deficit irrigation in maize. Agricultural Water Management, 2019; 212: 433–40.

[8] Zhang H, Han M, Comas L H, DeJonge K C, Gleason S M, Trout T J, et al. Response of Maize Yield Components to Growth Stage-Based Deficit Irrigation. Agronomy Journal, 2019; 111: 1–9. doi: 10.2134/agronj2019.03.0214

[9] Comas L H, Trout T J, Banks G T, Zhang H, DeJonge K C, Gleason S M. USDA-ARS Colorado maize growth and development, yield and water-use under strategic timing of irrigation, 2012-2013. Data in Brief, 2018.

[10] Trout T J, Bausch W C. USDA-ARS Colorado maize water productivity data set. Irrigation Science, 2017; 35: 241–249. doi: 10.1007/s00271-017-0537-9

[11] Trout T J, DeJonge K C. Crop water use and crop coefficients of maize in the great plains. Journal of Irrigation and Drainage Engineering, 2018; 144(6).

[12] DeJonge K C, Taghvaeian S, Trout T J, Comas L H. Comparison of canopy temperature-based water stress indices for maize. Agricultural Water Management, 2015; 156: 51–62.

[13] Han M, Zhang H, DeJonge K C, Comas L H, Trout T J. Estimating maize water stress by standard deviation of canopy temperature in thermal imagery. Agricultural Water Management, 2016; 177: 400–9.

[14] Kullberg E G, DeJonge K C, Chávez J L. Evaluation of thermal remote sensing indices to estimate crop evapotranspiration coefficients. Agricultural Water Management, 2016; 179: 64–73.

[15] Zhang H, Han M, Chávez J L, Lan Y. Improvement in estimation of soil water deficit by integrating airborne imagery data into a soil water balance model. International Journal of Agricultural and Biological Engineering, 2017; 10(3): 37–46.

[16] Han M, Zhang H, Chávez J L, Ma L, Trout T J, DeJonge K C. Improved soil water deficit estimation through the integration of canopy temperature measurements into a soil water balance model. Irrigation Science, 2018.

[17] Han M, Zhang H, DeJonge K C, Comas L H, Gleason S. Comparison of three crop water stress index models with sap flow measurements in maize. Agricultural Water Management, 2018; 203: 366–75.

[18] Gleason S M, Cooper M, Wiggans D R, Bliss C A, Romay M C, Gore MA, et al. Stomatal conductance, xylem water transport, and root traits underpin improved performance under drought and well-watered conditions across a diverse panel of maize inbred lines. Field Crops Research, 2019; 234: 119–28.

[19] Gleason S M, Wiggans D R, Bliss C A, Comas L H, Cooper M, DeJonge K C, et al. Coordinated decline in photosynthesis and hydraulic conductance during drought stress in Zea mays. Flora, 2017; 227: 1–9.

[20] Chávez J L, Zhang H, Capurro M C, Masih A, Altenhofen J, editors. Evaluation of multispectral unmanned aerial systems for irrigation management. SPIE Commercial + Scientific Sensing and Imaging; 2018: SPIE.

[21] Zhang L, Niu Y, Zhang H, Han W, Li G, Tang J, et al. Maize canopy temperature extracted from UAV thermal and RGB imagery and its application in water stress monitoring. Frontiers in plant science, 2019; 10: 1270.

[22] Zhang L, Zhang H, Niu Y, Han W. Mapping maize water stress based on UAV multispectral remote sensing. Remote Sensing, 2019; 11(6): 605.

[23] Niu Y, Zhang L, Zhang H, Han W, Peng X. Estimating above-ground biomass of maize using features derived from UAV-based RGB imagery. Remote Sensing, 2019; 11(11): 1261.

[24] Geipel J, Link J, Claupein W. Combined Spectral and Spatial Modeling of Corn Yield Based on Aerial Images and Crop Surface Models Acquired with an Unmanned Aircraft System. Remote Sensing, 2014; 6(11): 10335–55.

[25] Duan B, Fang S, Zhu R, Wu X, Wang S, Gong Y, et al. Remote estimation of rice yield with unmanned aerial vehicle (UAV) data and spectral mixture analysis. Frontiers in plant science, 2019; 10(204). doi: 10.3389/fpls.2019.00204

[26] Yan G, Li L, Coy A, Mu X, Chen S, Xie D, et al. Improving the

estimation of fractional vegetation cover from UAV RGB imagery by colour unmixing. ISPRS Journal of Photogrammetry and Remote Sensing, 2019; 158: 23–34.

[27] Allen R G, Walter I A, Elliott R, Howell T A, Itenfisu D, Jensen ME. The ASCE standardized reference evapotranspiration equation, Idaho, Task Committee on Standardization of Reference Evapotranspiration, 2005.

[28] Allen R G, Pereira L S, Raes D, Smith M. Crop Evapotranspiration-Guidelines for computing crop water requirements-FAO Irrigation and drainage paper 56. 1998; FAO, Rome 300: D05109.

[29] Jensen M E, Allen R G. Evaporation, evapotranspiration, and irrigation water requirements. ASCE Manuals and Reports on Engineering Practice, 2016; p. 1–767.

[30] Sakuratani T. A heat balance method for measuring water flux in the stem of intact plants. Journal of Agricultural Meteorology, 1981; 31: 9–17.

[31] USDA-NRCS. USDA-NRCS WEB soil survey. https://websoilsurvey.nrcs.usda.gov/app/HomePage.htm

[32] Scudiero E, Skaggs T H, Corwin D L. Regional-scale soil salinity assessment using Landsat ETM+ canopy reflectance. Remote Sensing of Environment, 2015; 169: 335–43.

[33] Rouse J W, Jr., Haas R H, Schell JA. Deering, D.W. Monitoring vegetation systems in the Great Plains with ERTS. In: Earth resources technology satellite-1 symposium, 3., 1973, Washington, DC. Proceedings… Washington, DC: NASA, 1973. p. 307–317.

[34] Huete A R. A soil-adjusted vegetation index (SAVI). Remote Sensing of Environment, 1988; 25: 295–309.

[35] Haboudane D, Miller J R, Tremblay N, Zarco-Tejada P J, Dextraze L. Integrated narrow-band vegetation indices for prediction of crop chlorophyll content for application to precision agriculture. Remote Sensing of Environment, 2002; 81(2): 416–26.

[36] Zhang Y J, Xie Z K, Wang Y J, Su P X, An L P, Gao H. Effect of water stress on leaf photosynthesis, chlorophyll content, and growth of oriental lily. Russian Journal of Plant Physiology, 2011; 58(5): 844.

[37] Klein R N, Shapiro CA. Evaluating hail damage to corn. University of Nebraska Lincoln Extension publications. http://extensionpublications.unl.edu/assets/pdf/ec126.pdf